REGULAR ARTICLE

blood advances

ASXL1 impairs osteoclast formation by epigenetic regulation of NFATc1

Nidhi Rohatgi,[1] Wei Zou,[1] Patrick L. Collins,[1] Jonathan R. Brestoff,[1] Timothy H. Chen,[2] Yousef Abu-Amer,[2] and Steven L. Teitelbaum[1,3]

[1]Department of Pathology and Immunology, [2]Department of Orthopedic Surgery, and [3]Division of Bone and Mineral Diseases, Department of Medicine, Washington University School of Medicine, St. Louis, MO

Key Points

- ASXL1 deletion in myeloid lineage cells promotes osteoclast differentiation resulting in low bone mass.
- ASXL1 modulates H3K27 methylation of osteoclastogenic gene promoters, including *NFATc1*.

Additional sex comb-like 1 (*ASXL1*) mutations are commonly associated with myeloid malignancies and are markers of aggressive disease. The fact that ASXL1 is necessary for myeloid differentiation raises the possibility it also regulates osteoclasts. We find deletion of ASXL1 in myeloid cells results in bone loss with increased abundance of osteoclasts. Because ASXL1 is an enhancer of trithorax and polycomb (ETP) protein, we asked if it modulates osteoclast differentiation by maintaining balance between positive and negative epigenetic regulators. In fact, loss of ASXL1 induces concordant loss of inhibitory H3K27me3 with gain of H3K4me3 at key osteoclast differentiation genes, including nuclear factor for activated T cells 1 (*NFATc1*) and *itgb3*. In the setting of ASXL1 deficiency, increased NFATc1 binds to the *Blimp1* (*Prdm1*) promoter thereby enhancing expression of this pro-osteoclastogenic gene. The global reduction of K27 trimethylation in ASXL1-deficient osteoclasts is also attended by a 40-fold increase in expression of the histone demethylase Jumonji domain-containing 3 (*Jmjd3*). Jmjd3 knockdown in ASXL1-deficient osteoclast precursors increases H3K27me3 on the *NFATc1* promoter and impairs osteoclast formation. Thus, in addition to promoting myeloid malignancies, ASXL1 controls epigenetic reprogramming of osteoclasts to regulate bone resorption and mass.

Introduction

Osteoclast is the bone-resorbing, myeloid lineage polykaryon. In keeping with its myeloid ontogeny, molecules which control myelopoiesis also regulate osteoclasts.

Osteoclast formation requires activation of RANK ligand (RANKL)/RANK signaling pathways including NF-κB and MAPKs such as extracellular signal-regulated kinase and p38.[1] These immediate signals result in synthesis of c-Fos, which collaborates with the key osteoclastogenic transcription factor, NFATc1, to autoactivate the latter's promoter thereby inducing osteoclastogenesis.[2] Although RANKL induces epigenetic changes that contribute to osteoclast formation, the mechanisms underlying this epigenetic remodeling in osteoclastogenesis still remain unclear.[3]

Additional sex comb-like (*ASXL*) genes encode enhancer of trithorax and polycomb (ETP) proteins, which, by facilitating histone methylation or demethylation, repress or stimulate gene transcription in a cell-specific context.[4,5] Transcriptional repression by ASXL proteins is mediated by recruiting polycomb receptor complex 2 (PRC2) to promoters, thereby increasing H3K27 methylation. Trimethylation of K27 results in gene inactivation, a process reversed by recruitment of a histone demethylase that removes H3K27me3 methyl groups.[6] These events also exist during osteoclastogenesis.[7]

An ASXL family gene, *ASXL2*, positively effects osteoclast formation as its deletion diminishes the number of bone resorptive cells, resulting in osteopetrosis.[8] Another member of the ASXL family, namely ASXL1, is associated with and dictates prognosis of a number of myeloid malignancies such as mastocytosis with associated myelodysplasia, which predisposes to osteoclast-dependent osteoporosis.[9,10]

Submitted 5 March 2018; accepted 18 August 2018. DOI 10.1182/bloodadvances.2018018309.

The full-text version of this article contains a data supplement.

Like ASXL2, ASXL1 also recognizes PPARγ, but whereas ASXL2 promotes adipogenesis, the process is arrested by ASXL1.[11]

Because ASXL1 suppresses the nuclear receptor (PPARγ), whose activity was presumed to promote physiological osteoclast formation, we postulated that specific deletion of *ASXL1* in myeloid lineage would induce the bone resorptive cell and diminish bone mass.[12] Although mice lacking ASXL1, exclusively in myeloid lineage cells, have low bone mass, their robust osteoclast formation is independent of canonical RANKL- and PPARγ-activated signals, including c-Fos expression. Like its induction of hematopoietic malignancies, however, the osteoclastogenic properties of ASXL1 deficiency involve demethylation of a repressive histone mark, H3K27me3. Consequently, the genes most affected by absence of ASXL1 are involved in osteoclast differentiation. A subset of these genes gain K4 trimethylation, a mark of active chromatin, and were enriched in NFAT-like motifs. One such gene is *prdm1* (*Blimp1*), the promoter of which exhibits increased binding to NFATc1 in knockout (KO) cells. The reciprocal increase in H3K4me3 on osteoclastic genes in ASXL1-deficient myeloid lineage cells may also be because of activation of the histone demethylase Jumonji domain-containing 3 (Jmjd3), which specifically removes K27 methyl groups from promoters. Thus, ASXL1 regulates osteoclast epigenome and its inactivation promotes bone loss.

Methods

Animals

All animals were housed in the animal care unit of Washington University School of Medicine, where they were maintained according to guidelines of the Association for Assessment and Accreditation of Laboratory Animal Care. All animal experimentation was approved by the Animal Studies Committee of Washington University School of Medicine.

Generation of ASXL1-deficient mice

Asxl1tm1a(EUCOMM)Wtsi were purchased from European Conditional Mouse Consortium. For deletion of the LacZ-neomycin-resistance cassette and for the generation of mice with LoxP-flanked *ASXL1* allele (*ASXL1*$^{f/+}$), those transmitting 100% were bred to *FLPo* (JAX mice 012930, C57BL/6 mice), which have transgenic expression of an enhanced form of the recombinase FLP driven by the GT(ROSA)26Sor promoter. ASXL1$^{f/+}$ mice were intercrossed to generate ASXL1$^{f/f}$ mice. ASXL1$^{fl/fl}$ mice generated were subsequently crossed with LysM-Cre mice (Jackson Laboratory). To fully delete ASXL1 using LysM-Cre, ASXL1$^{fl/fl}$, LysMCre$^{+/-}$ mice were crossed again to obtain animals bearing 2 copies of the LysM-Cre allele (ASXL1$^{fl/fl}$ LysMCre$^{+/+}$). LysMCre$^{+/+}$ and ASXL1$^{fl/fl}$ littermate without Cre mice served as control.

Macrophage isolation and osteoclast culture

All in vitro experiments were performed at least 3 times. Primary bone marrow macrophages (BMMs) were prepared as described[13] with slight modification. Marrow was extracted from femora and tibiae of 6- to 8-week-old mice with α minimum essential medium (α-MEM) and cultured in α-MEM containing 10% inactivated fetal bovine serum, 100 IU/mL penicillin, and 100 μg/mL streptomycin (α-10 medium) with 1:10 of mMCSF producing cell line, CMG 14-12 condition media on petri-plastic dishes. Cells were incubated at 37°C in 6% CO_2 for 3 days and then washed with phosphate-buffered saline (PBS) and lifted with 1× trypsin/EDTA in PBS. A total of 1.2×10^4 BMMs were cultured in 500 μL α-MEM containing 10% heat-inactivated fetal bovine serum with glutathione-S transferase–RANKL and 30 ng/mL of mouse recombinant macrophage colony-stimulating factor (M-CSF) in 48-well tissue culture plates, some containing sterile bovine bone slices. Cells were fixed and stained for tartrate-resistant acid phosphatase (TRAP) activity after 5 days in culture, using a commercial kit (Sigma 387-A; Sigma-Aldrich, St. Louis, MO). The images were captured using Nikon Eclipse E400 (Melville, NY) upright microscope.

Histone extraction, histone western blot

Histones were extracted by standard acid extraction protocol. Briefly, cells were lysed in triton extraction buffer (PBS containing 0.5% triton × 100 [vol/vol]) on ice for 10 minutes. The cells were centrifuged at 2000 rpm for 10 minutes followed by another wash with half the volume of triton extraction buffer. Pellet was resuspended in 0.2N HCl. Histones were acid extracted overnight at 4°C. The samples were centrifuged and supernatant removed. Protein was determined using Bradford assay.

Lentivirus infection

293-T cells were transfected with shJMJD3 together with a packaging plasmid (pHR0 8.2 δ R) and the envelope (pCMV-VSV-G) plasmid. After 48 hours, medium containing lentiviruses was collected and filtered. Macrophages obtained from 8- to 12-week-old male mice were infected with virus for 24 hours in the presence of 1:10 CMG and 10 μg/mL protamine (Sigma-Aldrich). Cells were selected in the presence of CMG and 1 μg/mL puromycin (Calbiochem) for 3 days before use as osteoclast precursors.

Chromatin immunoprecipitation (ChIP) assay

For immunoprecipitation, 60 μL of magnetic protein A beads were used. The beads were washed thrice with PBS containing 0.02% tween 20. After the final wash, beads were resuspended with the antibody overnight at 4°C. The next day, 1 to 2 million cells were plated in tissue culture plates (± RANKL). Formaldehyde was added directly to cell culture media for 10 minutes at room temperature such that the final concentration was 1%. Cross-linking was quenched by the addition of glycine to a final concentration of 0.125 M. Cells were washed 3 times with PBS, scraped off the plates in a small amount of PBS, and centrifuged, and the pellet was washed with PBS containing protease inhibitors (Complete, Roche). Cells were then resuspended in 1 mL PBS, and protease inhibitors centrifuged at 5000 rpm for 5 minutes at 4°C. The pellet was resuspended in cold sonication buffer (50 mM tris(hydroxymethyl)aminomethane [Tris]–HCl pH 8, 10 mM EDTA, 0.1% sodium dodecyl sulfate [SDS], 0.5% sodium deoxycholate and protease inhibitors) for 25 to 30 minutes on ice. Cells were aliquoted at 1×10^6 cells per mL concentration and chromatin sheared using Bioruptor (6 cycles, 10 minutes at high speed per cycle). The samples were centrifuged to pellet the cellular debris. Five percent of the cells were collected in a separate tube to be used as input control. The supernatant was divided equally between immunoprecipitation samples to include isotype control. Sheared DNA was incubated with the bead-antibody slurry. The next day, DNA-protein complexes were washed in low salt buffer (SDS 0.1%, Triton X100 1%, EDTA 2 mM, Tris-HCl pH 8.0 20 mM, NaCl 150 mM) followed by high salt buffer (SDS 0.1%, Triton X100 1%, EDTA 2 mM, Tris-HCl pH 8.0 20 mM, NaCl 500 mM), LiCl buffer (LiCl 0.25 M, nonidet P-40 1%, deoxycholate 1%, EDTA 1 mM, Tris-HCl pH 8.0, 10 mM), and Tris-EDTA buffer. DNA was eluted by adding 250 μL of elution buffer

(SDS 1%, NaHCO3 0.1 M). Samples and inputs were de-cross-linked and cleaned for quantitative polymerase chain reaction (qPCR) analysis.

Chromatin immunoprecipitation and DNA sequencing (ChIP-seq) and analysis

ChIP or input DNA was used for indexed library preparation (Illumina) and then subjected to 50-bp single-end sequencing per manufacturer's protocol on Illumina HiSeq3000. Sequenced libraries were aligned to the reference genome (mm10) using NovaAlign base settings. Peak calling was performed using MACS2.0 for H3K4me3 ChIP-seq[14] and HOMER for H3K27me3 ChIP-seq,[15] using paired inputs as peak calling controls. For heat maps and quantification of reads over peaks, genes, or promoter regions, reads per kilobase per million were extracted using Deeptools.[16] For log ratio (M) and average mean (A) (MA) plot analysis, reads were then further quantile normalized using the R package preprocessCore, prior to direct comparison. Direct visualization of ChIP-seq tracks was accomplished using the University of California, Santa Cruz Genome Browser.[17]

Statistics

Statistical significance was determined using multiple comparison in a 1-way or 2-way analysis of variance (ANOVA) test, or with unpaired nonparametric Student *t* test when only 2 groups were present, using GraphPad Prism v7 built-in statistical analysis (GraphPad Software Inc., La Jolla, CA). $P < .05$ was considered significant. All quantitative reverse transcription–PCR and qPCR data were expressed as mean from at least 3 independent biological experiments with at least 3 technical replicates.

Results

ASXL1 deletion in myeloid lineage cells promotes osteoclastogenesis resulting in low bone mass

To assess the influence of osteoclast differentiation on *ASXL1* expression, we cultured wild-type (WT) BMMs in the presence of RANKL and M-CSF and temporally measured ASXL1 messenger RNA (mRNA) and protein. Although the ETP gene was robustly expressed in naïve BMMs, abundance of its mRNA decreased approximately two-thirds within 24 hours of RANKL/M-CSF exposure with progressive decline as the osteoclast phenotype further matured (Figure 1A).

Because its expression declines with osteoclast differentiation, we postulated ASXL1 may negatively impact formation of the bone resorptive cell. We therefore conditionally deleted *ASXL1* in myeloid lineage cells by mating ASXL1$^{flox/flox}$ mice to those bearing lysozyme M Cre (ASXL1^{cKO}) leading to virtual arrested expression of the targeted gene (Figure 1B; supplemental Figure 1A). The conditionally deleted BMMs and their Cre- counterparts were cultured in osteoclastogenic conditions with increasing amounts of RANKL. After 5 days, the cells were stained for TRAP activity, and the number of osteoclasts was counted. Regardless of the amount of the osteoclastogenic cytokine, RANKL, ASXL1-deficient BMMs generated more osteoclasts than controls (Figure 1C-D). The abundance of ASXL1^{cKO} osteoclasts was confirmed by substantially greater expression of differentiation marker mRNA and protein, including NFATc1 (Figure 1E; supplemental Figure 1B). In contrast to its generation, the resorptive capacity of individual ASXL1^{cKO} osteoclasts was intact as manifested by their ability to organize their cytoskeleton to form actin rings and generate pits on bone (Figure 1F). In accordance, ASXL1$^{-/-}$ osteoclasts plated on bovine bone slices mobilized significantly more carboxy-terminal collagen (CTx), a marker of bone resorption than control cells (Figure 1G). Interestingly, RANKL- and M-CSF-stimulated classical osteoclastogenic signaling events in ASXL1^{cKO} BMMs were unaltered indicating other pathways were inducing the robust formation of the bone resorbing cell (supplemental Figure 1C-D). Reflecting our in vitro observations, μCT analysis established a 33% loss of trabecular bone volume and a 14% reduction of bone mineral density in ASXL1^{cKO} mice (Figure 2A-B). The number of osteoclasts were substantially enhanced in ASXL1^{cKO} femurs. In consequence, histomorphometrically determined trabecular bone volume was diminished (Figure 2C-D). Confirming robust osteoclastogenesis in ASXL1^{cKO} mice, serum analysis of Trap5B, a hallmark of osteoclast number, was elevated (Figure 2E). The decrease in bone mass did not reflect altered osteoblastogenesis as both osteoblast number per bone surface and P1NP serum levels remain unchanged (supplemental Figure 2A-B).

ASXL1^{cKO} osteoclast formation is not mediated by c-Fos or increased osteoclast progenitors

Although controversial, we reported that ASXL2 deletion dampens osteoclast formation by inactivating PPARγ.8 We therefore asked if absence of ASXL1 induced osteoclast differentiation in a reciprocal manner, namely, by stimulating the nuclear receptor, PPARγ. To determine if such is the case, we quantified the essential PPARγ osteoclastogenic target, c-Fos, which was modified by ASXL2.[8] Confirming the osteoclastogenic effect of ASXL1 deletion is likely not mediated by PPARγ, c-Fos expression was unaltered in RANKL/M-CSF–treated ASXL1^{cKO} BMMs (supplemental Figure 2C). Given the role of ASXL1 in the hematopoietic compartment,[18] we then asked if ASXL1 deletion with LysMcre may regulate hematopoiesis and osteoclast development. We found that the mice with ASXL1-deficient myeloid cells had normal bone marrow cellularity (supplemental Figure 3A) and exhibited no splenomegaly (supplemental Figure 3B). Fluorescence-activated cell sorter analysis of marrow also revealed that conditional myeloid deletion of ASXL1 did not alter frequencies or numbers of lineage negative, sca1 positive, c-kit negative (LSK), common myeloid progenitor, granulocyte/macrophage progenitor, megakaryocyte/erythroid progenitor, (supplemental Figure 3C) or RANK^{+} osteoclast progenitor cells (supplemental Figure 3D-E) in bone marrow. In addition, 5-bromo-2′-deoxyuridine incorporation established that proliferation of BMMs and preosteoclast was unaltered between the 2 genotypes (supplemental Figure 4A-B). To evaluate for possible hematopoietic defects, bone marrow cells were isolated from femurs of ASXL1$^{flox/flox}$ and ASXL1^{cKO} female mice (supplemental Figure 5A). Consistent with the progenitor data, we also found that frequencies and numbers of macrophages, Ly6C^{hi} monocytes, Ly6C^{lo} monocytes, neutrophils, CD19^{+} B cells, bulk CD3^{+} T cells, CD4^{+} T cells, CD8^{+} T cells, and CD4^{-}CD8^{-} T cells were unaltered in ASXL1^{cKO} mice (supplemental Figure 5B). Eosinophil frequencies and numbers (supplemental Figure 5B) were, however, slightly decreased in ASXL1^{cKO} bone marrow ($P < .05$). Erythrocyte frequencies and numbers (supplemental Figure 5C-D) were also similar in ASXL1$^{flox/flox}$ and ASXL1^{cKO} mice. Thus, conditional deletion of ASXL1 in myeloid lineage cells results in relatively specific hematopoietic alterations affecting osteoclasts and eosinophils but no other cell types, at least in mice ≤12 weeks of age.

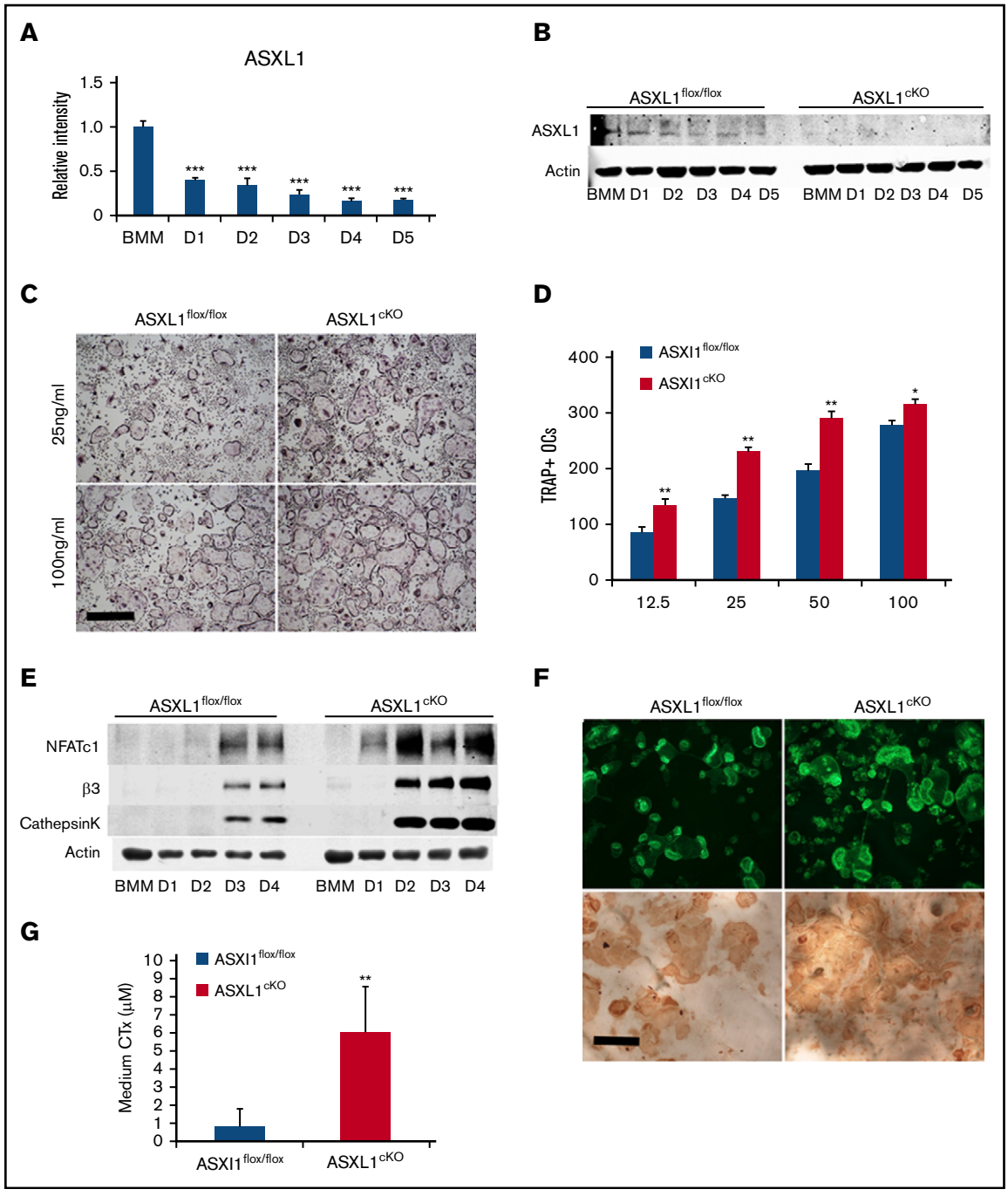

Figure 1. ASXL1 deletion in myeloid lineage cells promotes osteoclastogenesis. (A) Six- to 8-week-old WT BMMs were exposed to M-CSF and RANKL (50 ng/mL) for 5 days. *ASXL1* mRNA expression was determined by qPCR. One-way ANOVA was used to determine statistical differences. Data are represented as + standard deviation (SD). ***$P < .001$ relative to BMM control. (B) ASXL1$^{flox/flox}$ and ASXL1^{cKO} BMMs were cultured with M-CSF + RANKL (50 ng/mL) for 5 days. ASXL1 protein was determined by immunoblot. (C) Representative image showing ASXL1$^{flox/flox}$ and ASXL1^{cKO} BMMs cultured in M-CSF and RANKL (25 ng/mL and 100 ng/mL) for 5 days, after which cells were stained for TRAP activity. The images were captured using Nikon Eclipse E400 upright microscope. Scale bar represents 400 μm. (D) TRAP positive osteoclasts were then counted. Unpaired nonparametric Student *t* test was used to determine statistical differences. Error bars represent + SD; *$P < .05$, **$P < .01$ in comparison with their respective controls. (E) ASXL1$^{flox/flox}$ and ASXL1^{cKO} BMMs were cultured with M-CSF and RANKL (50 ng/mL) for 4 days. Total cell lysate was collected with time. Osteoclast differentiation proteins were determined by immunoblot. (F) ASXL1$^{flox/flox}$ and ASXL1^{cKO} BMMs were cultured with M-CSF and RANKL (100 ng/mL) on bovine bone slices. After 5 days, the cells were stained with Alexa-Fluor-546-phallodin to visualize the actin rings (top). The images were captured on the green channel of Nikon Eclipse E400 upright microscope. Following removal of the transduced osteoclasts, resorption pits were visualized by wheat germ agglutinin-lectin staining (bottom). Scale bar represents 100 μm. (G) ASXL1$^{flox/flox}$ and ASXL1^{cKO} BMMs were cultured with M-CSF and RANKL (100 ng/mL) for 6 days on bovine bone slices. Conditioned medium was assayed for CTx (6 bone slices were used for both genotypes). Error bars represent + SD; **$P < .01$. All experiments were conducted at least 3 times.

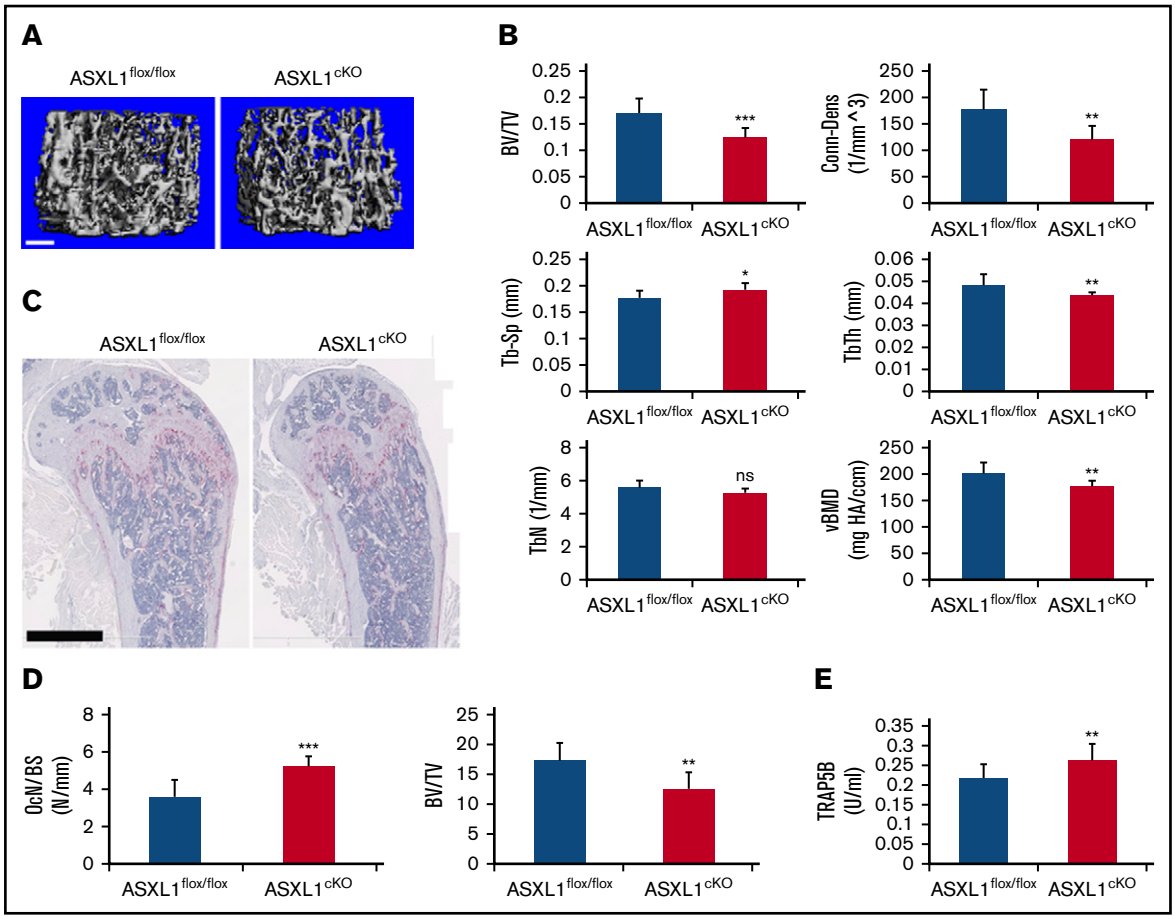

Figure 2. ASXL1^{cKO} mice have low bone mass. (A-B) Femurs of 13-week-old male ASXL1 $^{flox/flox}$ and ASXL1^{cKO} (ASXL1flox/flox LysM$^{cre/cre}$) littermates were subjected to μCT analysis (n = 5 in each group). Scale bar represents 100 μm. (C-D) Femurs of ASXL1$^{flox/flox}$ and ASXL1^{cKO} mice (left) stained for TRAP activity (red reaction product). Scale bar represents 1 mm. Histomorphometric analysis of osteoclast number (OcN) per bone surface (BS) and ratio of trabecular bone volume (BV) to total marrow space (total volume [TV]) of ASXL1$^{flox/flox}$ and ASXL1^{cKO} mice (n = 5 in each group) quantified using BioQuant software. (E) Serum analysis for TRAP5B in ASXL1$^{flox/flox}$ and ASXL1^{cKO} 12-week-old male mice (n = 7 mice in each group). Unpaired nonparametric Student *t* test was used for statistical analysis. Error bars represent + SD; *$P < .05$, **$P < .01$, ***$P < .001$. BV/TV, bone volume fraction of marrow; Conn-Dens, connectivity density, normed by TV; ns, not significant; TbN, trabecular number; TbSp, trabecular separation; TbTh, trabecular thickness; vBMD, volumetric bone mineral density.

ASXL1 deficiency alters H3K27me3 methylation of gene promoters

ASXL1 depletion leads to a marked reduction in genome-wide H3K27me3 in hematopoietic cells altering target gene expression.[18] We therefore asked if K27 trimethylation was altered in osteoclast lineage ASXL1^{cKO} cells such that ASXL1 deletion may have activated relevant genes. Like myeloid malignancies, bulk H3K27 methylation in fact was diminished in ASXL1-deficient preosteoclasts (Figure 3A). To identify genes regulated by these events in osteoclasts, we performed ChIP-seq. As a functional readout of ASXL1 activity, we used H3K27me3 and H3K4me3 antibodies to measure relative levels of transcriptional repression and promoter activation, respectively, in ASXL1$^{flox/flox}$ and ASXL1^{cKO} osteoclasts. As observed in the immunoblot, ChIP-seq data also revealed a global reduction in K27 trimethylation in the KO osteoclast. Of 25 321 H3K27me3 peaks found in either genotype, WT had fivefold more unique peaks than KO cells (Figure 3B, left panel). In addition, analysis of H3K27me3 levels across all genes (Figure 3B, right panel shows chromosome 1) indicated a global trend for loss of total H3K27me3. Gene-specific loss of H3K27me3 was supported by analyzing read coverage over all genomic features, which revealed a shift from promoter reads in WT cells to distal intragenic reads in the KO cells (Figure 3C).

Given chromosome-wide depletion of H3K27me3, we asked if genes most affected by ASXL1 loss were specific to osteoclast development. A total of 663 genes in KO osteoclast exhibited significant loss of K27 methylation (criteria used was greater than twofold change between the 2 groups). Of these, Gene Set Enrichment Analysis revealed significant enrichment of osteoclast differentiation pathway as well as transcriptional regulation (Figure 3D; supplemental Figure 6). Thus, although KO of ASXL1 broadly impacted the H3K27me3 epigenome of osteoclasts, we could identify subsets of genes that may be specifically regulated by ASXL1.

As loss of ASXL1 resulted in promoter-specific depletion of H3K27me3, we analyzed for concordant loss of H3K27me3 with gain of the promoter histone modification H3K4me3. MA plots document K27 methylation of the key osteoclastic genes, *NFATc1*,

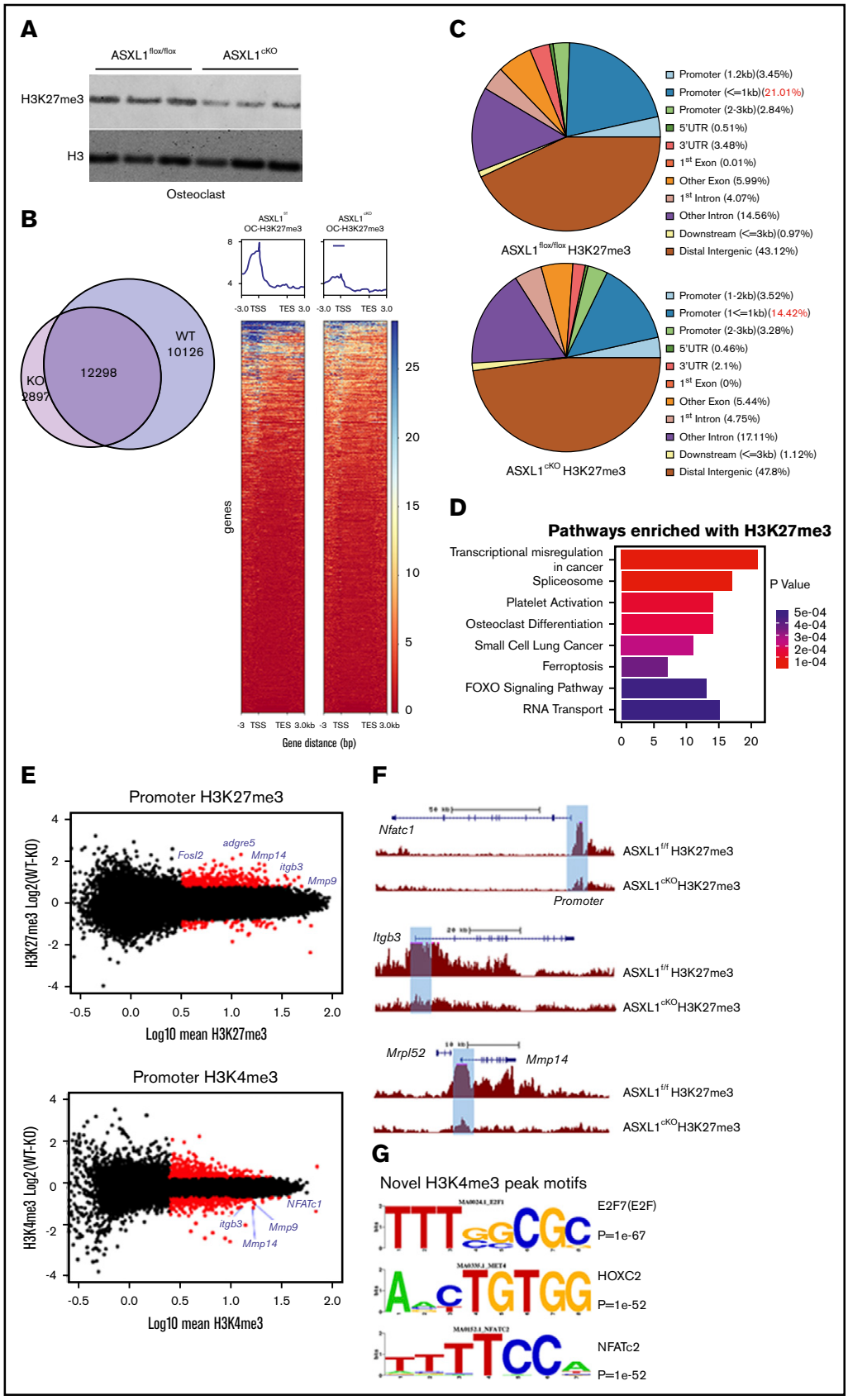
A
ASXL1 flox/flox
ASXL1 cKO
H3K27me3
H3
Osteoclast
B
WT
10126
KO
2897
12298
ASXL1 wt OC-H3K27me3
ASXL1 cKO OC-H3K27me3
-3.0 TSS TES 3.0
genes
-3 TSS TES 3.0kb
Gene distance (bp)
C
Promoter (1.2kb)(3.45%)
Promoter (<=1kb)(21.01%)
Promoter (2-3kb)(2.84%)
5'UTR (0.51%)
3'UTR (3.48%)
1st Exon (0.01%)
Other Exon (5.99%)
1st Intron (4.07%)
Other Intron (14.56%)
Downstream (<=3kb)(0.97%)
Distal Intergenic (43.12%)
ASXL1 flox/flox H3K27me3
Promoter (1-2kb)(3.52%)
Promoter (1<=1kb)(14.42%)
Promoter (2-3kb)(3.28%)
5'UTR (0.46%)
3'UTR (2.1%)
1st Exon (0%)
Other Exon (5.44%)
1st Intron (4.75%)
Other Intron (17.11%)
Downstream (<=3kb) (1.12%)
Distal Intergenic (47.8%)
ASXL1 cKO H3K27me3
D
Pathways enriched with H3K27me3
Transcriptional misregulation in cancer
Spliceosome
Platelet Activation
Osteoclast Differentiation
Small Cell Lung Cancer
Ferroptosis
FOXO Signaling Pathway
RNA Transport
P Value
5e-04
4e-04
3e-04
2e-04
1e-04
E
Promoter H3K27me3
H3K27me3 Log2(WT-KO)
Log10 mean H3K27me3
Fosl2
adgre5
Mmp14
itgb3
Mmp9
Promoter H3K4me3
H3K4me3 Log2(WT-KO)
Log10 mean H3K4me3
NFATc1
F
Nfatc1
Promoter
Itgb3
Mrpl52
Mmp14
ASXL1 f/f H3K27me3
ASXL1 cKO H3K27me3
G
Novel H3K4me3 peak motifs
E2F7(E2F)
P=1e-67
HOXC2
P=1e-52
NFATc2
P=1e-52

Figure 3.

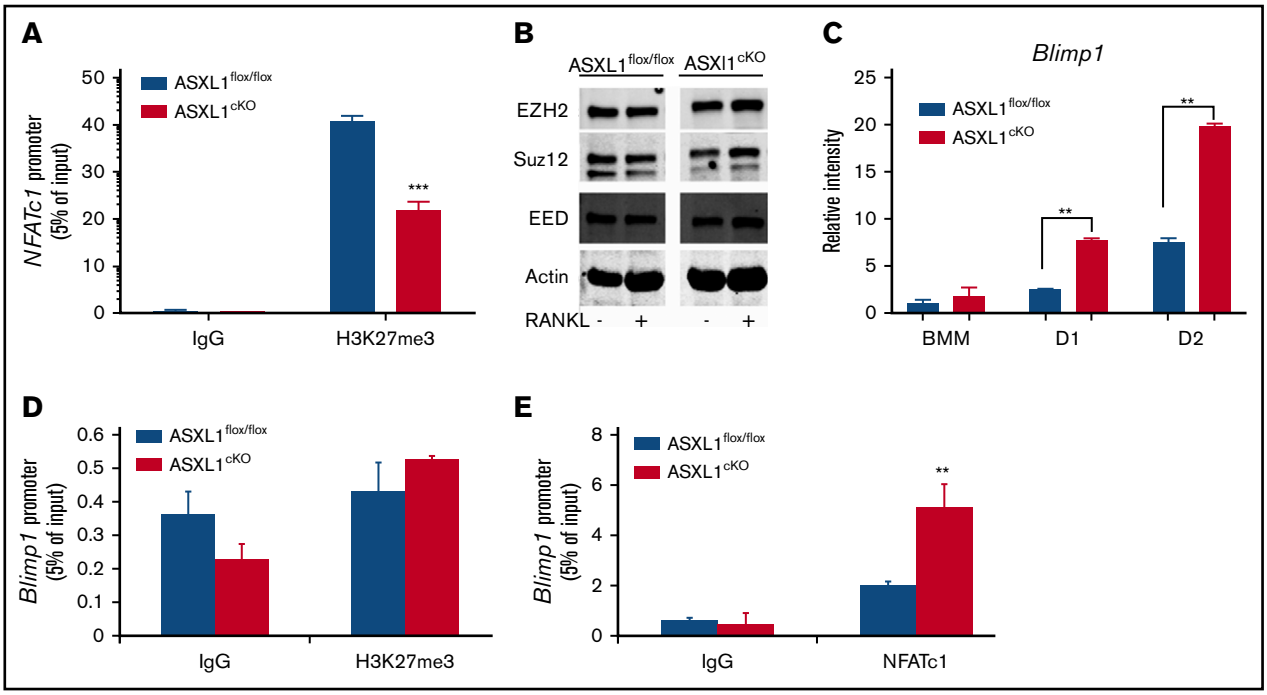

Figure 4. Increased pro-osteoclastogenic transcription factors in ASXL1-deficient osteoclasts. (A) ASXL1$^{flox/flox}$ and ASXL1^{cKO} BMMs were exposed to M-CSF and RANKL (50 ng/mL) for 2 days. H3K27me3 binding to NFATc1 response element in the *NFATc1* promoter was determined by ChIP assay. Immunoglobulin G (IgG) served as a control. (B) ASXL1$^{flox/flox}$ and ASXL1^{cKO} BMMs were cultured in M-CSF and RANKL (50 ng/mL) for 1 day. PRC proteins were determined by immunoblot. Actin served as loading control. (C) ASXL1$^{flox/flox}$ and ASXL1^{cKO} BMMs were cultured in the presence of M-CSF and RANKL (50 ng/mL). RNA was harvested on days 1 and 2 of RANKL stimulation, and *Blimp1* mRNA abundance was determined by qPCR. (D) ASXL1$^{flox/flox}$ and ASXL1^{cKO} BMMs were exposed to M-CSF and RANKL (50 ng/mL) for 2 days. H3K27me3 binding to *Blimp1* promoter was determined by ChIP assay. IgG served as control. (E) ASXL1$^{flox/flox}$ and ASXL1^{cKO} BMMs were exposed to M-CSF and RANKL (50 ng/mL) for 2 days. NFATc1 binding to *Blimp1* promoter was determined by ChIP assay. IgG served as control. n = 3 independent experiments from 10- to 12-week-old male mice. Two-way ANOVA was used for statistical analysis. Error bars represent + standard error of the mean; $^{**}P < .01$, $^{***}P < .001$.

itgb3, *Mmp9*, and *Mmp14* to have increased K27 methylation in the ASXL1$^{flox/flox}$ in comparison with KO (Figure 3E, top). On the other hand, alterations of K4 methylation, an indicator of active chromatin, were much less dramatic on some of these gene promoters (Figure 3E, bottom). Importantly, K27 methylation on promoters upstream of TSS of specific genes such as *NFATc1*, *itgb3*, and *Mmp14* visualized using University of California, Santa Cruz Genome Browser was decreased (Figure 3F). These observations raised the possibility that depletion of ASXL1 de-represses transcription factors that drive the formation of new H3K4me3 positive promoters. To identify these potential regulatory pathways, we performed a motif enrichment analysis of novel H3K4me3 peaks specific to the ASXL1^{cKO} cells. Utilizing de novo motif prediction, and a highly stringent statistical cut off ($P < 1e\text{-}50$), we identified enrichment of NFAT-like motifs in the KO promoters (P value =1e-52) (Figure 3G; supplemental Tables 1 and 2). ASXL1^{cKO} osteoclast lineage cells exhibit specific loss of H3K27me3 with gain of H3K4me3 at the *NFATc1* promoter, along with genome-wide enrichment of NFAT motifs in the novel ASXL1-KO promoters.

Increased pro-osteoclastogenic transcription factors in ASXL1-deficient osteoclasts

Additional ChIP-qPCR using H3K27me3 antibody validated the ChIP-seq observation that H3K27me3 enrichment of the *NFATc1* promoter was markedly reduced in ASXL1^{cKO} osteoclasts (Figure 4A). This observation, taken with NFAT enrichment on actively transcribing genes in KO cells, indicated the enhanced osteoclast formation attending cell-autonomous ASXL1 deficiency represents demethylation of NFATc1-residing H3K27me3.

Figure 3. ASXL1 deficiency alters H3K27me3 methylation on gene promoters. (A) ASXL1$^{flox/flox}$ and ASXL1^{cKO} BMMs from 12-week-old male mice were cultured with M-CSF and 50 ng/mL RANKL for 2 days. Representative immunoblot of bulk histone methylation for H3K27me3 on acid extracted histones. Total H3 was used as a loading control (n = 3 independent experiments). (B) ASXL1$^{flox/flox}$ (WT) and ASXL1^{cKO} (KO) osteoclast were chromatin immunoprecipitated using H3K27me3 or H3K4me3 antibody followed by DNA sequencing. Model based analysis of ChIP-seq data (MACS2) for H3K27me3 methylation. Left: Venn diagram made with http://jolars.co/eulerr/. Right: Heat map for H3K27me3 on chr1 in ASXL1$^{flox/flox}$ and ASXL1^{cKO} osteoclast (+3 kb of transcription start site [TSS]). (C) Characterization of H3K27me3 binding sites in various genomic regions in ASXL1$^{flox/flox}$ and ASXL1^{cKO} osteoclasts. (D) Gene sets uniquely enriched in KO mice with H3K27me3 loss using Kyoto Encyclopedia of Genes and Genomes pathway analysis. (E) MA plots for H3K27me3 (up) and H3K4me3 (down) to visualize genes (data points) that are being identified as differentially bound (red). Osteoclast relevant genes identified in blue. (F) H3K27me3 peaks at individual loci (highlighted blue bar), *NFATc1*, *itgb3*, and *Mmp14*; WT (ASXL1$^{flox/flox}$) and KO (ASXL1^{cKO}). (G) Motif enrichment analysis of novel H3K4me3 binding sites in ASXL1^{cKO} osteoclasts.

ASXL1 regulates transcription by interacting with PRC2, which includes EZH2, Suz12, and EED.[19] Thus, ASXL1 deficiency may alter the PRC2 complex proteins, thereby attenuating H3K27me3 methylation. For example, robust osteoclastogenesis attending ASXL1 deficiency may represent an abundance of EZH2, which delivers methylated H3K27 to the promoter of *Irf8*, thereby silencing its osteoclast-inhibiting properties.[20] To explore this possibility, we measured PRC2 proteins in ASXL1^{cKO} macrophages and osteoclastic cells. Despite decreased H3K27me3 methylation in ASXL1^{cKO} osteoclasts, expression of PRC2 core members in mutant BMMs was unchanged, even as they underwent osteoclast differentiation (Figure 4B). *Blimp1* (encoded by *Prdm1*[21]), an established positive regulator of osteoclastogenesis, and a transcriptional repressor of antiosteoclastogenic genes, increased in ASXL1-KO osteoclasts (Figure 4C). In contrast to *NFATc1*, however, H3K27me3 on *Blimp1* promoter was not significantly different between the control and KO osteoclasts (Figure 4D), indicating absence of ASXL1 likely did not exert its Blimp1 inductive effect directly by regulating histone methylation. Consistent with previous reports that NFATc1 regulates *Blimp1* expression,[17] ASXL1-deletion markedly enhanced NFATc1 occupancy on the *Blimp1* promoter (Figure 4E).

Loss of H3K27me3 in ASXL1-deficient osteoclasts is mediated by JMJD3

The loss of K27 methylation in ASXL1^{cKO} osteoclasts could likely be because of removal of methyl groups from the lysine residues on histone H3, by a demethylase specific to K27 trimethylation,[22] Jmjd3. The effects of ASXL1 loss on H3K27me3 occupancy raised the possibility of whether K27 methylation on the *Jmjd3* promoter was also altered. However, H3K27me3 on the *Jmjd3* promoter near the TSS was unchanged. Although its significance is enigmatic, K27 methylation of promoter elements further upstream was decreased (Figure 5A). In addition, we found expression of *Jmjd3* increased 40-fold in ASXL1-deficient osteoclasts (Figure 5B). Fortifying its relevance to ASXL1-deficient osteoclastogenesis, Jmjd3 knockdown in ASXL1^{cKO} BMMs (supplemental Figure 7) also restored H3K27me3 methylation on osteoclastogenic gene promoters, including *NFATc1* and *Blimp1* (Figure 5C-D). Consequently, Jmjd3 knockdown specifically in KO osteoclasts also prevented expression of both NFATc1 and *Blimp1* (Figure 5E). This decrease in pro-osteoclastogenic genes with Jmjd3 knockdown further arrested osteoclast formation (Figure 5F). Thus, ASXL1 negatively regulates osteoclastogenesis by altering histone methylation on osteoclast gene promoters (Figure 6).

Discussion

ASXL1 mutations in patients with systemic mastocytosis and associated clonal hematologic non–mast-cell disease induce osteoporosis.[10] However, the relationship between osteoclasts and myeloid leukemias, particularly those with inactivating ASXL1 mutations, which profoundly compromise survival, is enigmatic.[9] ASXL1 is indispensable to myeloid differentiation, and we find mice bearing ASXL1-deficient myeloid precursors form more osteoclasts than their littermate controls resulting in low bone mass. Surprisingly, the enhanced osteoclastogenesis of ASXL1^{cKO} mice is not characterized by activation of IκBα, extracellular signal-regulated kinase, and other MAPKs, which typically attend RANKL and M-CSF signaling. Although the changed osteoclast number may also reflect precursor abundance or apoptosis of the mature polykaryon, we found marrow cell abundance is unaltered, with no changes in the hematopoietic progenitor population. This is consistent with previous literature that establishes osteoclasts are not required for hematopoietic stem cell maintenance and mobilization.[23]

Like ASXL2, ASXL1 recognizes PPARγ, but in contrast to the negative consequences of ASXL2 deletion, lack of ASXL1 promotes adipogenesis, at least in vitro.[8,11] In addition to its effects on lipid and insulin homeostasis, PPARγ is postulated to be an essential component of the osteoclastogenic process, and we demonstrated that ASXL2$^{-/-}$ mice have a paucity of osteoclasts and are osteopetrotic.[8,12] We established, however, that although PPARγ mediates thiazolidinedione-stimulated osteoclast formation, its absence does not alter osteoclast abundance in physiological and pathological circumstances.[24] This observation challenged our conclusion that the osteopetrosis of ASXL2$^{-/-}$ mice reflects inactivation of PPARγ and prompted us to explore alternative signaling pathways whereby ASXL1 deletion stimulates formation of the bone resorptive cell. The present study also indicates that osteoclastogenic effects of ASXL1 deletion are not indicative of PPARγ activity. This conclusion rests on the lack of effect of ASXL1 deletion on expression of c-Fos, which is the directly induced key mediator whereby PPARγ promotes osteoclast formation in response to thiazolidinediones.[12] Despite absence of c-Fos induction, typically a central event inducing NFATc1, expression of the latter is enhanced in ASXL1$^{-/-}$ osteoclast lineage cells.

The unaltered expression or activation of classical osteoclastogenic signaling molecules, including MAPKs, IκBα, and c-Fos, suggests that the increased osteoclast differentiation resulting from ASXL1 deletion reflects an alternative mechanism such as epigenetic regulation. This conclusion is in keeping with the established capacity of ASXL1 to enhance or suppress gene expression by altering histone methylation in a gene- and cell-specific manner. In the absence of ASXL1, genes are demethylated, and its repressive activity arrested. In fact, suppression of PRC2 recruitment is a likely means by which ASXL1 mutations contribute to the pathogenesis of aggressive myeloid malignancies.[18] This suggests that epigenetic mechanisms may also mediate osteoclastogenic effects of associated with ASXL1 deletion. We found a reduction in bulk H3K27 trimethylation in ASXL1-deficent osteoclast lineage cells. This observation prompted us to determine expression of candidate genes that regulate osteoclast formation by modifying histone methylation. EZH2 is a key component of PRC2, which promotes osteoclast formation by suppressing the inhibitor Irf8.[20] Thus, we expected enhanced EZH2 in ASXL1^{cKO} osteoclasts but observed a diminution, suggesting PRC2 members are not central to epigenetic modifications in the conditionally deleted animals promoting their abundance of osteoclasts.

Blimp 1 is a transcriptional repressor that promotes osteoclast differentiation by reducing inhibitors such as Irf8 and Mafb.[21] Because it is transduced by NFATc1, we asked if Blimp1 is a possible mediator of ASXL1 deficiency–induced osteoclast formation. The substantial increase in *Blimp1* mRNA in ASXL1-deficient osteoclasts, in the absence of altered H3K27me3 methylation, indicates that *Blimp1* (*Prdm1*) transactivation is directly induced by abundant, epigenetically stimulated NFATc1 binding to its promoter.

Involvement of H3K27me3 demethylase provides another likely explanation for increased *Blimp1* in ASXL1-deficient osteoclasts. Jmjd3 is an H3K27me3 demethylase that inhibits somatic cell reprogramming by enhancing P16^{INK4a} [25] and may undergo a

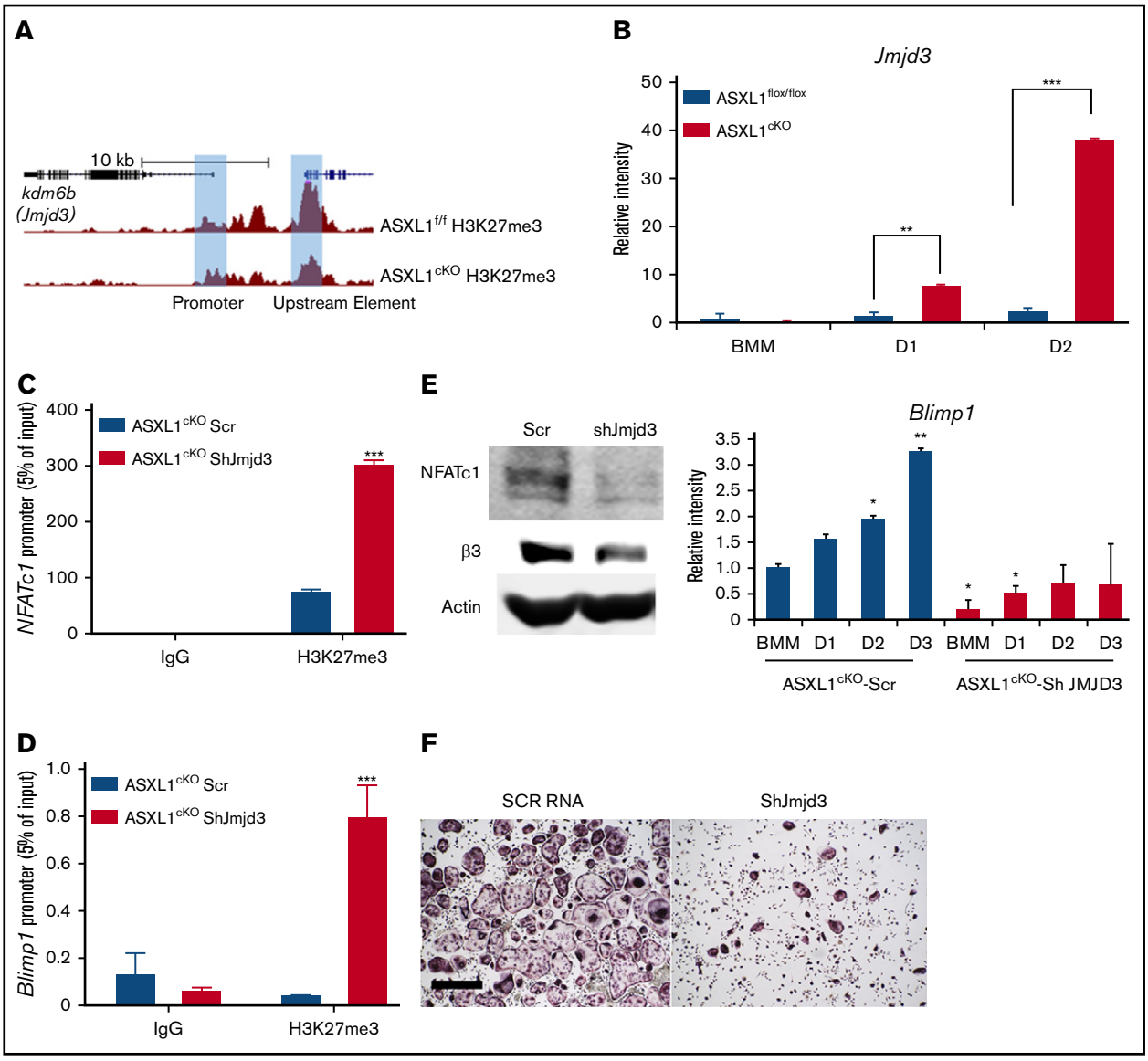

Figure 5. Loss of H3K27me3 in ASXL1-deficient osteoclasts is mediated by Jmjd3. (A) H3K27me3 peaks at individual loci (highlighted blue bar) on *Jmjd3* promoter; WT (ASXL1$^{flox/flox}$) and KO (ASXL1^{cKO}). (B) ASXL1$^{flox/flox}$ and ASXL1^{cKO} BMMs were cultured in the presence of M-CSF and RANKL (25 ng/mL). RNA was harvested on days 1 and 2 of RANKL stimulation, and histone H3 Lys 27 (H3K27) demethylase *Jmjd3* mRNA abundance was determined by qPCR. Unpaired nonparametric Student *t* test was used for statistical analysis. Error bars represent + SD; $^{**}P < .01$, $^{***}P < .001$. (C-D) ASXL1^{cKO} BMMs, transduced with scr or Jmjd3 short hairpin RNA (shRNA), were exposed to M-CSF and RANKL (25 ng/mL) for 2 days. H3K27me3 binding to *NFATc1* promoter (C) and *Blimp1* promoter (D) was determined by ChIP assay. IgG served as control. n = 2 independent experiments from 10- to 12-week-old male mice. Two-way ANOVA was used for statistical analysis. Error bars represent + standard error of the mean; $^{***}P < .001$. (E) ASXL1^{cKO} BMMs, transduced with scr or Jmjd3 shRNA, were exposed to M-CSF and + RANKL for 3 days. Expression of osteoclast differentiation proteins NFATc1 and β3 integrin was determined by immunoblot (left) and *Blimp1* by qPCR (right). n = 3 independent experiments from 8-week-old male mice. One-way ANOVA was used for statistical analysis. Error bars represent + SD; $^{*}P < .05$, $^{**}P < .01$. (F) ASXL1^{cKO} BMMs, transduced with scr or shRNA for Jmjd3, were exposed to M-CSF and + RANKL for 5 days and stained for TRAP activity. Images were captured on Nikon Eclipse E400. Scale bar represents 400 μm.

PRC2-mediated epigenetic switch.[26] Although regulation of JMJD3 is enigmatic, its capacity to demethylate H3K27me3 on the *NFATc1* promoter and thus stimulate osteoclast formation is established.[7] We find *Jmjd3* expression markedly enhanced in ASXL1^{cKO} cells, and its knockdown arrests their increased osteoclastogenesis by promoting H3K27me3 methylation on bone resorptive genes. The size of the ASXL1 gene (~6 kb) compromised overexpressing ASXL1 in KO cells and directly assessing its role in regulating Jmjd3, which will be a future goal. Nonetheless, our study establishes that ASXL1 regulates osteoclast epigenome via expression of *Jmjd3*, which demethylates H3K27m3 on the *NFATc1* promoter increasing its sensitivity to RANKL. Enhanced NFATc1 in turn binds to and activates pro-osteoclastogenic genes such as *Blimp1*.

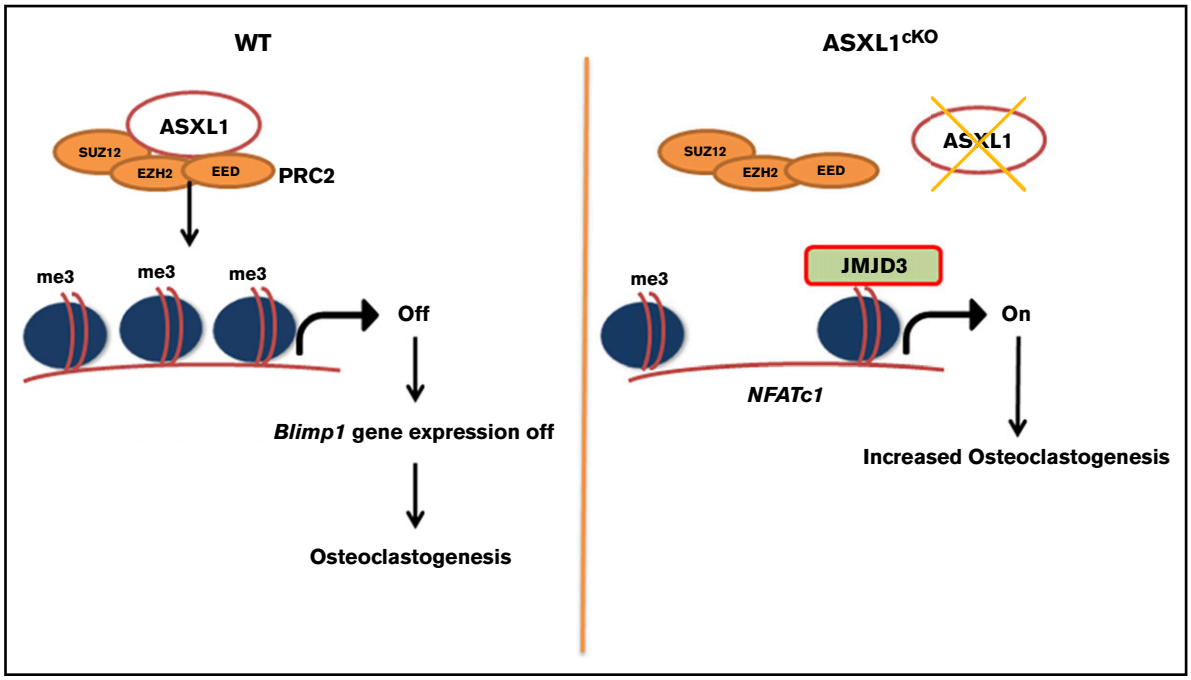

Figure 6. Schematic representation for role of ASXL1 in regulating osteoclastogenesis. ASXL1 binds to PRC2 proteins to methylate promoters of key osteoclast differentiation genes such as *NFATc1* and regulate their expression (left). Absence of ASXL1 prevents PRC2-mediated histone methylation (right). Jmjd3, specific demethylase for H3K27me3 in turn removes K27 methyl groups from promoters such as *NFATc1*, resulting in increased osteoclastogenesis.

Although the relationship between myeloid linage cells and osteoclasts is established, these findings show that mutations promoting hematopoietic malignancies may also directly modulate osteoclast formation. Thus, the osteoclastogenesis of ASXL1 deficiency does not involve classical RANKL- or M-CSF-stimulated molecules such as MAPKs and c-Fos but activation of NFATC1 by reversal of suppressive histone methylation. Epigenetic modification of myeloid lineage genes is therefore central to skeletal homeostasis and may participate in malignancy associated bone loss.

Acknowledgments

The authors thank Genome Technology Access Center at Washington University for performing ChIP-seq and providing technical assistance.

This work was supported by grants from the National Institute of Arthritis and Musculoskeletal and Skin Diseases, National Institutes of Health (R37 AR046523 [S.L.T.], R01 AR054326 [Y.A.-A.], R01 AR072623 [Y.A.-A.], and P30 AR057235 [S.L.T. and Y.A.-A.]); the National Institute of Diabetes and Digestive and Kidney Diseases, National Institutes of Health (grant R01 DK111389) (S.L.T.); and Shriners Hospitals for Children (grant 85400-STL) (S.L.T.).

Authorship

Contribution: N.R. designed and performed experiments and wrote the manuscript; W.Z. and J.R.B. designed and performed experiments; P.L.C. performed experiments and edited the manuscript; T.H.C. performed experiments; Y.A.-A. designed experiments; and S.L.T. designed experiments and wrote the manuscript.

Conflict-of-interest disclosure: The authors declare no competing financial interests.

Correspondence: Steven L. Teitelbaum, Department of Pathology and Immunology, Washington University School of Medicine, Campus Box 8118, 660 South Euclid Ave, St. Louis, MO 63110; e-mail: teitelbs@wustl.edu.

References

1. Novack DV, Teitelbaum SL. The osteoclast: friend or foe? *Annu Rev Pathol*. 2008;3(1):457-484.
2. Asagiri M, Sato K, Usami T, et al. Autoamplification of NFATc1 expression determines its essential role in bone homeostasis. *J Exp Med*. 2005;202(9):1261-1269.
3. Nishikawa K, Iwamoto Y, Kobayashi Y, et al. DNA methyltransferase 3a regulates osteoclast differentiation by coupling to an S-adenosylmethionine-producing metabolic pathway. *Nat Med*. 2015;21(3):281-287.
4. Baskind HA, Na L, Ma Q, Patel MP, Geenen DL, Wang QT. Functional conservation of Asxl2, a murine homolog for the Drosophila enhancer of trithorax and polycomb group gene Asx. *PLoS One*. 2009;4(3):e4750.
5. Gildea JJ, Lopez R, Shearn A. A screen for new trithorax group genes identified little imaginal discs, the Drosophila melanogaster homologue of human retinoblastoma binding protein 2. *Genetics*. 2000;156(2):645-663.

6. Margueron R, Reinberg D. The Polycomb complex PRC2 and its mark in life. *Nature*. 2011;469(7330):343-349.

7. Yasui T, Hirose J, Tsutsumi S, Nakamura K, Aburatani H, Tanaka S. Epigenetic regulation of osteoclast differentiation: possible involvement of Jmjd3 in the histone demethylation of Nfatc1. *J Bone Miner Res*. 2011;26(11):2665-2671.

8. Izawa T, Rohatgi N, Fukunaga T, et al. ASXL2 regulates glucose, lipid, and skeletal homeostasis. *Cell Reports*. 2015;11(10):1625-1637.

9. Seitz S, Barvencik F, Koehne T, et al. Increased osteoblast and osteoclast indices in individuals with systemic mastocytosis. *Osteoporos Int*. 2013;24(8): 2325-2334.

10. Damaj G, Joris M, Chandesris O, et al. ASXL1 but not TET2 mutations adversely impact overall survival of patients suffering systemic mastocytosis with associated clonal hematologic non-mast-cell diseases. *PLoS One*. 2014;9(1):e85362.

11. Park UH, Yoon SK, Park T, Kim EJ, Um SJ. Additional sex comb-like (ASXL) proteins 1 and 2 play opposite roles in adipogenesis via reciprocal regulation of peroxisome proliferator-activated receptor gamma. *J Biol Chem*. 2011;286(2):1354-1363.

12. Wan Y, Chong LW, Evans RM. PPAR-gamma regulates osteoclastogenesis in mice. *Nat Med*. 2007;13(12):1496-1503.

13. Lam J, Takeshita S, Barker JE, Kanagawa O, Ross FP, Teitelbaum SL. TNF-alpha induces osteoclastogenesis by direct stimulation of macrophages exposed to permissive levels of RANK ligand. *J Clin Invest*. 2000;106(12):1481-1488.

14. Zhang Y, Liu T, Meyer CA, et al. Model-based analysis of ChIP-Seq (MACS). *Genome Biol*. 2008;9:R137.

15. Heinz S, Benner C, Spann N, et al. Simple combinations of lineage-determining transcription factors prime cis-regulatory elements required for macrophage and B cell identities. *Mol Cell*. 2010;38(4):576-589.

16. Ramírez F, Ryan DP, Grüning B, et al. deepTools2: a next generation web server for deep-sequencing data analysis. *Nucleic Acids Res*. 2016;44(W1): W160-W165.

17. Karolchik D, Baertsch R, Diekhans M, et al; University of California Santa Cruz. The UCSC Genome Browser Database. *Nucleic Acids Res*. 2003;31(1): 51-54.

18. Abdel-Wahab O, Adli M, LaFave LM, et al. ASXL1 mutations promote myeloid transformation through loss of PRC2-mediated gene repression. *Cancer Cell*. 2012;22(2):180-193.

19. Abdel-Wahab O, Dey A. The ASXL-BAP1 axis: new factors in myelopoiesis, cancer and epigenetics. *Leukemia*. 2013;27(1):10-15.

20. Fang C, Qiao Y, Mun SH, et al. Cutting edge: EZH2 promotes osteoclastogenesis by epigenetic silencing of the negative regulator IRF8. *J Immunol*. 2016;196(11):4452-4456.

21. Nishikawa K, Nakashima T, Hayashi M, et al. Blimp1-mediated repression of negative regulators is required for osteoclast differentiation. *Proc Natl Acad Sci USA*. 2010;107(7):3117-3122.

22. Hong S, Cho YW, Yu LR, Yu H, Veenstra TD, Ge K. Identification of JmjC domain-containing UTX and JMJD3 as histone H3 lysine 27 demethylases. *Proc Natl Acad Sci USA*. 2007;104(47):18439-18444.

23. Miyamoto T. Role of osteoclasts in regulating hematopoietic stem and progenitor cells. *World J Orthop*. 2013;4(4):198-206.

24. Zou W, Rohatgi N, Chen TH, Schilling J, Abu-Amer Y, Teitelbaum SL. PPAR-γ regulates pharmacological but not physiological or pathological osteoclast formation. *Nat Med*. 2016;22(11):1203-1205.

25. Zhao W, Li Q, Ayers S, et al. Jmjd3 inhibits reprogramming by upregulating expression of INK4a/Arf and targeting PHF20 for ubiquitination. *Cell*. 2013; 152(5):1037-1050.

26. Shi X, Zhang Z, Zhan X, et al. An epigenetic switch induced by Shh signalling regulates gene activation during development and medulloblastoma growth. *Nat Commun*. 2014;5:5425.